Available online at www.sciencedirect.com
ScienceDirect
Proceedings of the Combustion Institute 32 (2009) 3059–3066
Proceedings of the Combustion Institute
www.elsevier.com/locate/proci

Experimental and numerical investigations of flame pattern formations in a radial microchannel

Aiwu Fan [a,b], Sergey Minaev [c], Evgeniy Sereshchenko [c], Roman Fursenko [c], Sudarshan Kumar [d], Wei Liu [b], Kaoru Maruta [a,*]

[a] *Institute of Fluid Science, Tohoku University, Katahira 2-1-1, Aoba-ku, Miyagi, Sendai 980-8577, Japan*
[b] *School of Energy and Power Engineering, Huazhong University of Science and Technology, Wuhan 430074, China*
[c] *Institute of Theoretical and Applied Mechanics, SB RAS, Novosibirsk 630090, Russia*
[d] *Aerospace Engineering Department, IIT Bombay, Powai, Mumbai 400076, India*

Abstract

Flame pattern formations in a heated radial microchannel with a gap width of 1.75 mm were investigated experimentally and numerically. A premixed methane–air mixture was introduced at the center of microchannel formed by two parallel quartz discs which were heated with an external porous burner to create a positive temperature gradient condition in the direction of flow. In addition to conventional stable flames, some non-stationary flame patterns termed single- and double-pelton-like flames and the traveling flame were also observed. The double- and single-pelton-like flames occurred at a random possibility under certain conditions, which rotated around the center of the radial microchannel at a frequency of ~25–55 Hz. Regime diagram of all those flame patterns was drawn based on the experimental findings in the mixture equivalence ratio range of 0.65–1.30 and inlet mixture velocity range of 1.5–5.0 m/s. Meanwhile, the experimental results also qualitatively verify our previous theoretical prediction that is the S-shaped dependency of flame radial location on inlet velocity for stoichiometric mixture. Finally, numerical simulations using a global one-step Arrhenius reaction model successfully captured some rotating flame structures that may be associated with single- and double-pelton-like flames observed in the experiments.

Keywords: Micro-combustion; Radial microchannel; Pattern formation; Flame instability; Rotating flame

1. Introduction

Combustions at micro- and meso-scales have received extensive interest in the past decade due to up to 100 times higher energy densities of hydrocarbon fuels as compared with those of the conventional electrochemical batteries [1,2]. However, the increased heat loss due to large surface area-to-volume ratio [3,4] and the wall radical quenching [4] make it difficult to achieve a stable and efficient combustion under reduced scales. Therefore, thermal management, for instance, heat recirculation [5], is frequently adopted in the design of microscale combustors [6–8]. In this technique, fresh mixture is preheated by the burned hot gas through solid walls. The "Swill roll" combustor is a good example of burners with heat recirculation which has been implemented to stabilize flame in micro- and meso-scales burners

* Corresponding author. Fax: +81 22 217 5311.
E-mail address: maruta@ifs.tohoku.ac.jp (K. Maruta).

1540-7489/$ - see front matter © 2009 The Combustion Institute. Published by Elsevier Inc. All rights reserved.
doi:10.1016/j.proci.2008.06.092

[6–8]. Many efforts were made to understand fundamentals of micro- to meso-scale combustion with heat recirculation. For example, Ju and coworker [9,10] observed fast and slow burning regimes and spinning flames in meso-scale channels. Miesse et al. [11,12] and Prakash et al. [13] found various diffusion flame modes such as multiple discrete flame cells in Y-shaped micro-combustors. Richecoeur and Kyritsis [14] investigated flame oscillations with sound emission in curved meso-scale ducts. Experiments in miniaturized liquid-film combustor by Sirignano et al. [15] demonstrated externally and internally anchored flame modes. Pham et al. [16] proposed that the liquid-film flame is composed of a double flame at the exit rim and a central triple flame within the chamber. This theory was supported by their chemiluminescence measurements of OH, CH, and C2 intensities.

In our group, Maruta et al. [17,18] have studied the combustion behavior of premixed CH_4/air mixtures in a heated quartz tube with a 2.0-mm diameter. In their investigations, a stable premixed flame was found to exist at high and low mixture velocities. At moderate velocities, three unstable flame propagation modes: (a) pulsating flame, (b) flames with repetitive extinction and ignition (FREI) and (c) a combination of pulsating and FREI modes were observed.

Later, Kumar et al. [19–21] performed experimental investigations on flame dynamics in a heated radial microchannel using premixed CH_4/air mixtures. This configuration can be used as a combustion chamber in micro power generation devices or systems, such as disk-type micro gas turbines [22], e.g., the MIT micro gas turbine. In addition to conventional stable circular flame, various non-stationary flame patterns, such as rotating pelton-like flame (this is termed since flame shape resembles a Pelton-wheel [19–21]), traveling flame, and so forth, were observed. More recently, Fan et al. [23,24] extended the mixture equivalence ratio to a much wider range. Some new flame patterns were observed and the regime diagrams of those flame patterns in the radial microchannels with a gap width of 0.5, 1.0, 1.5, 2.0, 2.5 and 3.0 mm were drawn based on their experimental findings. Those regime diagrams present a clear overview of the relation between each flame pattern and the experimental parameters, such as the inlet mixture velocity, the mixture equivalence ratio and the channel gap width.

Theoretical analyses by Minaev et al. reveal that in both 1D straight [25] and 2D radial [26,27] microchannel flames are unstable if the values of inlet gas velocities lie in a range of moderate velocities. At high inlet velocities normal stable flames exist, while at low inlet velocities weak stable flames with reduced flame temperatures are predicted. It is also demonstrated that the flame location versus inlet mixture velocity (flow rate) exhibits an S-shaped curve for stoichiometric mixture, as shown in Fig. 1 for the 2D radial microchannel [27]. The theoretical analysis [25] qualitatively agrees with our experimental findings in the 1D straight microchannel [18]. It is noteworthy that the weak stable flames were observed by camera with CH filter and a long enough exposure time, e.g., 1200 s. For the case of 2D radial microchannel, some previous experimental data for the stoichiometric mixtures are shown in Fig. 2. From this figure it can be seen that when the channel gap width is 1.0 mm, only non-stationary flames, i.e., pelton-like flame and traveling flame are observed. When the channel gap width is increased to 1.5 mm, only at low inlet velocity, e.g. 1.5 m/s, stable flame locates near the inlet of the radial microchannel. It is not the weak stable flame as that observed in the 1D straight microchannel. While in the 2.0-mm-gapped channel, all the flames are stable. Therefore, the S-shaped curve has not been verified by our previous experiments so far. However, from Fig. 2 it can be expected that the S-shaped curve would be confirmed by the experiment in the radial microchannel with a gap width between 1.5 and 2.0 mm, e.g., 1.75 mm.

On the other hand, flame dynamics, such as FREI, have been numerically confirmed by Jackson et al. [28] in the 1D straight microchannel and by Pizza et al. [29] in 2D planar microchannel. However, none of the flame patterns observed in our 2D radial microchannel has been captured by numerical simulations to date. Thus, in the present work, we first report the experimental observations of flame pattern formations in the heated radial microchannel with a gap width of

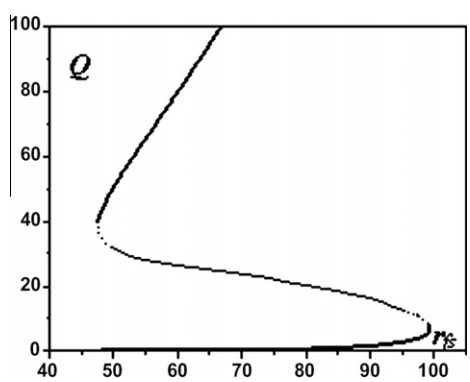

Fig. 1. The dependency of non-dimensional flow rate Q on non-dimensional flame radius r_{fs} evaluated for a radial channel with sub-critical gap, with r_{fs} in units of Dth/U_b (Dth is the gas thermal diffusivity and U_b is the adiabatic flame speed) and Q in units of Dth. Bold, dashed and dotted lines denote stable, unstable and pulsating branches of the $Q(r_{fs})$ curve respectively. Details of this figure could be found in [27].

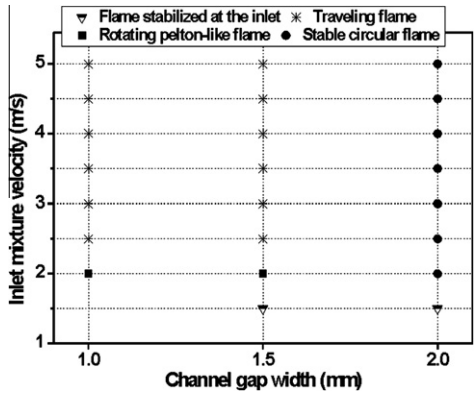

Fig. 2. Flame pattern regime diagram of stoichiometric mixture.

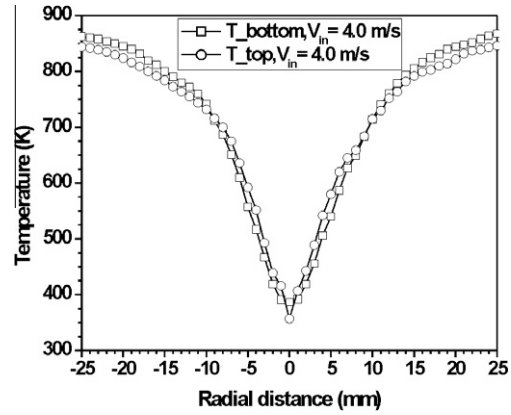

Fig. 4. Wall temperature profiles at an inlet airflow velocity of 4.0 m/s.

1.75 mm, and then present the numerical simulation results that may be associated with rotating pelton-like flames using a global one-step Arrhenius reaction model.

2. Experimental

2.1. Experimental setup and method

A schematic diagram of the experimental setup is shown in Fig. 3. Two circular quartz plates (ϕ 50) were maintained parallel to each other within an accuracy of $\pm 0.1°$. The gap between the two plates is 1.75 mm. The channel is heated from bottom by a porous burner with constant heat input. Before fuel supply, wall temperature profiles were created by using cold airflow. This approach was also employed in the series of previous studies [17–21,23,24]. Figure 4 shows the typical wall temperature profiles at an inlet airflow velocity of 4.0 m/s. The flow rates of gases were monitored through electric mass flow controllers within an accuracy of $\pm 1\%$. Methane–air mixture was injected at the center of the top plate through a delivery tube (ϕ4). In order to maintain a laminar flow in the delivery tube, the maximal mixture velocity at the delivery tube was set at 5.0 m/s, where the representative Reynolds number is ~1300. Movie recordings of various flame patterns were carried out with an image-intensified high-speed video camera right after the mixture was ignited in the microchannel. Other details about the experimental method could be found elsewhere [19–21,23,24].

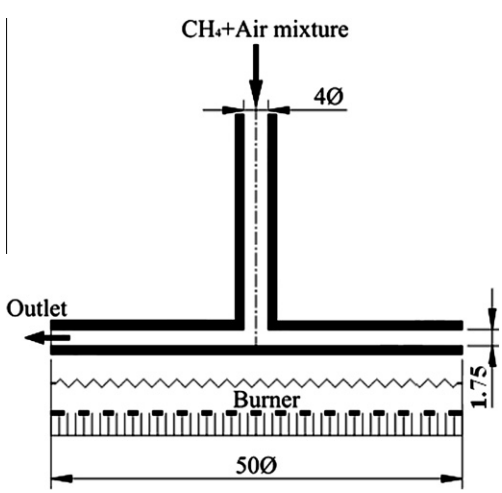

Fig. 3. Schematic diagram of the experimental setup.

2.2. Experimental results

Three different flame patterns, i.e., stable circular flame, single and double pelton-like flames, and traveling flame were observed in the experiments, as shown in Fig. 5a–d. From Fig. 5a it is seen that the circular flame front is a stable, symmetric circle with uniform luminosity. The radial location of the circular flame increases with increasing inlet mixture velocity for the same equivalence ratio. When the inlet mixture velocity keeps constant, radius of the circular flame reaches its minimum at equivalence ratio of about unity. The pelton-like flames rotate around the central axis of the radial microchannel at a frequency of ~25.0–55.0 Hz which depends on both mixture equivalence ratio and inlet mixture velocity. When the inlet mixture velocity keeps constant, the rotating frequency of the pelton-like flame reaches its maximum at an equivalence ratio ~1.0–1.05. This implies that the rotating frequency has a positive relation with the burning velocity. For the same mixture equivalence ratio, the rotating frequency decreases with increasing inlet mixture velocity. The double- and single-pel-

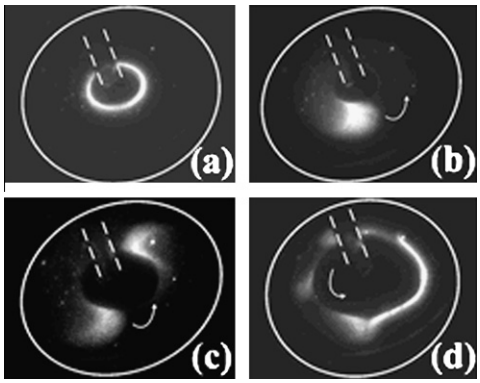

Fig. 5. One shot photos of different flame patterns taken with an image-intensified high-speed video camera at a rate of 500 frames per second with a shutter speed of 1/500 s from a top-side viewpoint: (a) stable circular flame, (b) single pelton-like flame, (c) double pelton-like flame, and (d) traveling flame. Solid and dashed white lines indicate the positions of top plate and mixture delivery tube, respectively. Arrows were drawn to indicate the rotating direction of the rotating flame patterns.

ton-like flames occurred at a random possibility under certain conditions, which demonstrates that this reactive flow system exhibits some bifurcation in flame pattern formation in those cases. The traveling flame looks like a closed circle with non-uniform luminosity with the naked eyes. However, with the help of an image-intensified high-speed video camera, it can be seen that a pelton-like flame cell emanates from one end of the luminous flame and travels towards the opposite end. At the moment of its approach, the opposite end of the luminous flame also generates a pelton-like flame cell which merges with the approaching one. This merger can be clearly seen in Fig. 5d. Another major characteristic of the traveling flame is the relatively loud sound emission. We suppose that it is produced at the moment those two pelton-like flame cells merge with each other in opposite rotating directions.

Regime diagram of these flame patterns was also obtained and presented in Fig. 6. Experiments were conducted under all the conditions denoted by the nodes in Fig. 6. The nodes without symbols in the figure mean that no flame was observed under those conditions. From Fig. 6 we can see that flame pattern formations are almost symmetrically distributed on the lean and rich sides. The distributions of the rotating pelton-like flame and the traveling flame in the regime diagram look like two horizontal C-shaped letters. From Fig. 6, it is evident that the flame pattern formation is a function of the inlet mixture velocity and mixture equivalence ratio. Let's now examine the dependency of flame pattern formation on the inlet mixture velocity for the stoichiometric mixtures. When the inlet mixture velocity, $V_{in} = 3.5$–5.0 m/s, circular flames stabi-

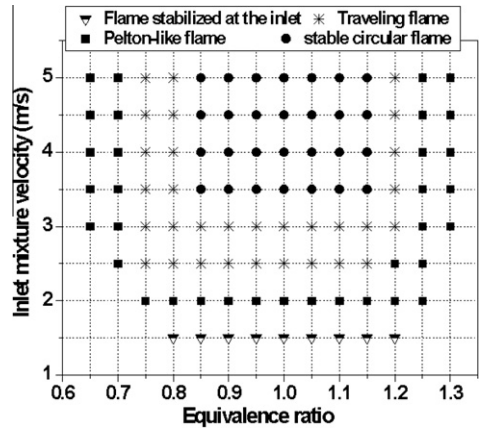

Fig. 6. Regime diagram of flame patterns for the radial microchannel with a gap width of 1.75 mm.

lized at certain radial locations. As the inlet mixture velocity reduced to $V_{in} = 3.0$–2.0 m/s, non-stationary flame patterns, i.e., the traveling flames and the rotating pelton-like flame appeared. At even lower inlet mixture velocity, $V_{in} = 1.5$ m/s, flame was seen to be stabilized near the inlet of the radial microchannel. This flame is geometrically similar to a deformed Bunsen flame due to the constraint of the narrow channel gap. As pointed out earlier, this flame is not the weak stable flame predicted by the theoretical solution [27]. Therefore, it is out of our interest here. Due to the extremely low luminosity of the weak flame and the interference of the flame of the heating burner, weak flame at very low inlet velocity has not been observed in the radial microchannel yet. Nevertheless, our experimental findings, as discussed above and shown in Fig. 7, qualitatively confirmed the upper and middle branches of the S-shaped curve predicted by the analytical solution for the stoichiometric mixtures [27]. We consider

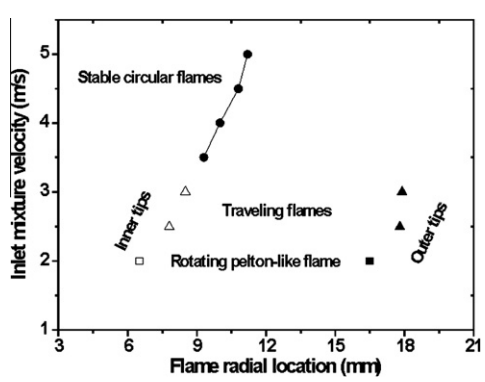

Fig. 7. Flame radial location versus inlet mixture velocity in the radial microchannel with a gap width of 1.75 mm for the stoichiometric flames.

that the pelton-like flame and the traveling flames have an analogy to the flames with repetitive extinction and ignition (FREI) in the 1D case [18,25].

Measurements of exhaust gas revealed that the stable flames can achieve a nearly complete combustion, while for the cases of the traveling flame and the rotating pelton-like flame, relatively large amount of unburned fuel leakages were detected due to the unclosed flame configurations. Details about the combustion completeness and chemical efficiency of various flame patterns are addressed elsewhere [24].

3. Numerical simulation

As discussed in [27], according to the simplified model assuming infinitely thin zone of chemical reaction, the non-dimensional flame radial location of stoichiometric mixture, r_{fs}, depends on non-dimensional gas flow rate and typical $Q(r_{fs})$ dependency looks like an S-shaped curve. The upper part of the curve lying above upper turning point is associated with normal flame. The intermediate branch of the S-shaped curve corresponds to unstable solution. There is also a low velocity mode of combustion described by the branch lying below lower turning point. This regime is stable and is characterized by small values of inlet gas flow velocities and reduced flame temperature. An attempt of description of some non-stationary 2D structures has been done in [26] in the frame of weak non-linear flame front model. The results of that analytical study showed the existence of periodical traveling waves within the velocities interval relating to the unstable branch of the S-shaped curve. Thus, we examine the rotating pelton-like flames in this velocity interval in the following numerical simulations.

As our aim here is to qualitatively capture the rotating pelton-like flame structures, it would be expensive to apply a model with full chemistry. Therefore, we assume a global one-step Arrhenius reaction, constant transport properties, and a constant density approximation. The gas-phase temperature T, the mass fractions of fuel Y_f and oxidizer Y_o variations are described by

$$\rho c_p\left(\frac{\partial T}{\partial t}+(\vec{V}\cdot\nabla)T\right)=\lambda\Delta T-\frac{2\alpha}{d}(T-\theta)+QW(Y_o,Y_f,T) \quad (1)$$

$$\frac{\partial(\rho Y_o)}{\partial t}+(\vec{V}\cdot\nabla)(\rho Y_o)=D\Delta(\rho Y_o)-\nu W(Y_o,Y_f,T) \quad (2)$$

$$\frac{\partial(\rho Y_f)}{\partial t}+(\vec{V}\cdot\nabla)(\rho Y_f)=D\Delta(\rho Y_f)-W(Y_o,Y_f,T) \quad (3)$$

where

$$W(Y_o,Y_f,T)=\rho A Y_o^a Y_f^b\exp(-E/RT) \quad (4)$$

is the chemical reaction rate and we chose $A=5\times10^8\ \mathrm{s}^{-1}$, $E/R=15{,}042$ K, $a=1.65$, $b=0.1$, $\rho=1.3\ \mathrm{g\,m^{-3}}$, $c_p=1000\ \mathrm{J\,kg^{-1}\,K^{-1}}$, $\lambda=0.026\ \mathrm{J\,K^{-1}\,m^{-1}\,s^{-1}}$, $D=2\times10^{-5}\ \mathrm{m^2\,s^{-1}}$, $Q/c_p=33{,}000$ K and $\nu=3.62$ that is the ratio of stoichiometric coefficients. The α in Eq. (1) is the heat transfer coefficient related to the Nusselt number by $Nu=\alpha d/\lambda$, where d is the channel gap width which is less than the critical value corresponding to the stoichiometric mixture and room temperature of the channel. For simplicity we set $Nu=4$. The convective and diffusion terms in Eqs. (1)–(3) read in polar coordinates (r, ϕ), where r is radius and ϕ is angle, as follows:

$$(\vec{V}\cdot\nabla)=\frac{G}{r}\frac{\partial}{\partial r},\quad \Delta=\frac{1}{r}\frac{\partial}{\partial r}\left(r\frac{\partial}{\partial r}\right)+\frac{1}{r^2}\frac{\partial^2}{\partial\varphi^2} \quad (5)$$

The formula (5) implies existence of axially symmetric radial flow with radial gas velocity G/r, where $G=V_0r_0$, V_0 is the input gas velocity and r_0 is the inlet radius.

The computation domain is a ring $r_0<r<R_0$ and we set $r_0=2\times10^{-3}$m and $R_0=0.04$ m that roughly correspond to the experimental configuration. It is assumed that the profile of channel wall temperature, θ, is time-constant and it is determined by formulae

$$\theta=T_0+(\Theta-T_0)\frac{r-r_0}{r_1-r_0}\quad \text{for } r_0<r<r_1$$

and

$$\theta=\Theta\quad \text{for } r_1<r<R_0 \quad (6)$$

where $r_1=0.025$ m, and $\Theta=900$ K that approximates the experimental profile.

The boundary conditions for the inlet and exit are set as follows:

At the inlet ($r=r_0$)

$$T=T_0,\quad Y_f=Y_f^0,\quad Y_o=Y_o^0 \quad (7)$$

while at the exit ($r=R_0$) zero flux conditions for Y_o, Y_f and T are applied, i.e.

$$\nabla T=\nabla Y_f=\nabla Y_o=0 \quad (8)$$

In the course of numerical simulations we set that initial profile of gas temperature as that described by formula (6) and it is coincided with temperature distribution in the wall. The choice of initial concentrations profiles depend on the value of inlet velocity related to parameter G by Eq. (5).

Numerical integrations of the non-stationary Eqs. (1)–(3) were carried out by an implicit finite-difference scheme. Accuracy of the solution method was tested by preliminary trials with different space grids and time steps. We used grid with 1500 (radial points) × 350 (angular points) nodes. At the first stage of numerical calculations

we evaluated the unstable interval of gas velocity by using Eqs. (1)–(3) in the case of radial symmetry ($\partial T/\partial\varphi = 0$, $\partial Y_o/\partial\varphi = 0$, $\partial Y_f/\partial\varphi = 0$). At the next stage we simulated evolution of initial distributions of concentrations and temperatures at fixed value of parameter G determining the inlet gas velocity. If the value of gas velocity was larger than maximal value of unstable interval of the S-shaped curve, any initial distributions transformed into circular stationary flame. This result corroborates with results of analytical studies [26,27]. In the case of small values of $G = 0.001\ \mathrm{m^2\,s^{-1}}$ we started from initial distribution of concentrations describing by formulas

$$Y_o = Y_o^0, \quad Y_f = Y_f^0, \text{ for } r_0 < r \leqslant r_b - r_b\frac{\varphi}{2\pi}$$

and

$$Y_o = 0, \quad Y_f = 0, \text{ for } r > r_b - r_b\frac{\varphi}{2\pi} \tag{9}$$

where $r_b = 0.03$ m.

Numerical simulations reveal that after ignition the flame acquired pelton-like shape and it rotates around central axis of radial microchannel. The distributions of fuel concentration in sequenced points of time with time steps about 0.017 are shown in Fig. 8, from which we can see that there is some leakage of unburned fuel. This was verified by the measurement of exhaust gas conducted in [23,24]. The gas temperature distributions at the same moments are given in Fig. 9, which are geometrically similar to the rotating pelton-like flames observed in the experiments. It is interesting that the flame shape is not fixed and slightly changes during its rotation and the flame edge located near the centre of rotation circumscribes a crooked path. We found that an increase of parameter G (e.g. $G = 0.0015\ \mathrm{m^2\,s^{-1}}$) led to a possibility of existence of two rotating flame cells resembling double pelton-like flames. The temperature distributions in sequenced points of time with time steps about 0.016 s are shown in Fig. 10. The flame luminosity strongly depends on temperature, so, roughly speaking, the domains filled by combustion products is visible only if their temperatures exceed some critical value. To make clear the qualitative comparison we marked by black color the regions with gas temperature less than 900 K. It is important that resulting configuration of rotating flames is independent of ini-

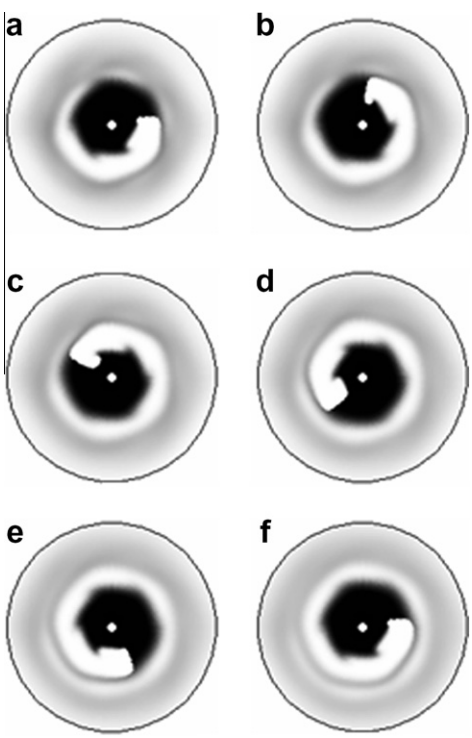

Fig. 8. Distribution of fuel concentration in sequenced points of time when $G = 0.001\ \mathrm{m^2/s}$. Gray shades correspond to different concentrations. The black domain marks region filled by unburned mixture and white color corresponds to absence of fuel. White circle in the centre marks the delivery tube.

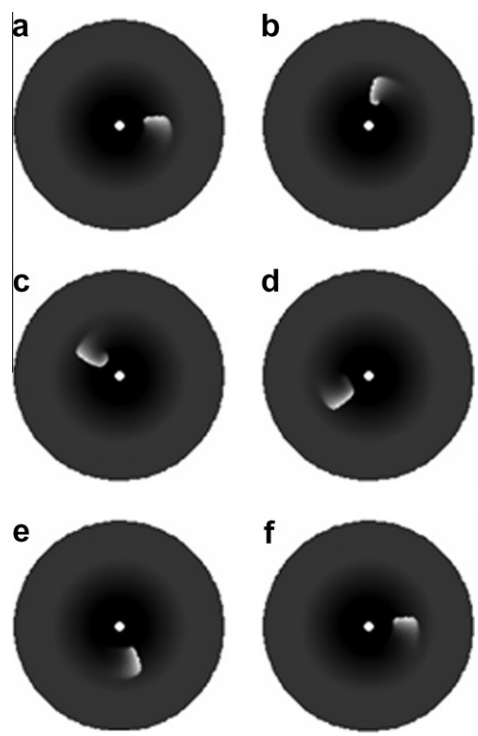

Fig. 9. Distribution of temperature in sequenced points of time when $G = 0.001\ \mathrm{m^2/s}$. Gray shades correspond to different temperatures. The black domain marks region filled by gas with temperature less than 900 K. White circle in the centre marks the delivery tube.

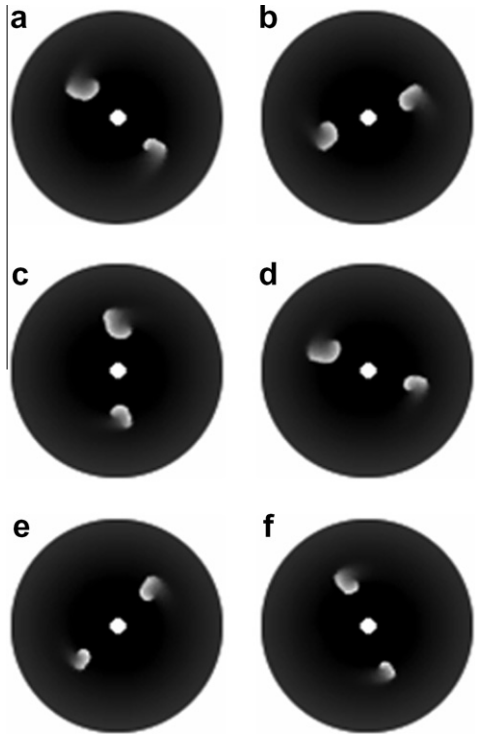

Fig. 10. Distribution of temperature in sequenced points of time when $G = 0.0015\ m^2/s$. Gray shades correspond to different temperatures. The black domain marks region filled by gas with temperature less than 900 K. White circle in the centre marks the delivery tube.

tial distribution and it is defined by the value of input gas velocity.

4. Conclusions

We reported the experimental observations of flame pattern formations in a heated radial microchannel. In addition to conventional stable circular flame, single- and double-rotating-pelton-like flames, and traveling flame were also observed with the help of an image-intensified high-speed video camera. Those flame pattern formations are functions of the inlet mixture velocity and the mixture equivalence ratio. The present experiments partly verified our previous analytical solution [27], with the exception of the weak flame that has not been observed yet. The middle branch of the S-shaped curve represents unstable solutions. Within the velocity interval of this branch, we carried out numerical simulation using a global one-step Arrhenius reaction model. Rotating structures that may be associated with single- and double-pelton-like flames observed in the experiments were successfully captured.

Acknowledgments

The authors thank Mr. S. Hasegawa, Mr. Y. Tsuboi, Dr. T. Yokomori, Dr. H. Yang and Dr. H. Nakamura of IFS, Tohoku University for help in conducting the present experiment and for instructive discussions.

References

[1] A.C. Fernandez-Pello, *Proc. Combust. Inst.* 29 (2002) 883–899.
[2] J. Vican, B.F. Gajdeczko, F.L. Dryer, D.L. Milius, I.A. Aksay, R.A. Yetter, *Proc. Combust. Inst.* 29 (2002) 909–916.
[3] T.T. Leach, C.P. Cadou, *Proc. Combust. Inst.* 30 (2005) 2437–2444.
[4] S. Raimondeau, D. Norton, D.G. Vlachos, R.I. Masel, *Proc. Combust. Inst.* 29 (2002) 901–907.
[5] S.A. Lloyd, F.J. Weinberg, *Nature* 251 (1974) 47–50.
[6] F.J. Weinberg, P.D. Ronney, *Proc. Combust. Inst.* 29 (2002) 941–947.
[7] C.H. Kuo, P.D. Ronney, *Proc. Combust. Inst.* 31 (2007) 3277–3284.
[8] N.I. Kim, S. Kato, T. Kataoka, et al., *Combust. Flame* 141 (3) (2005) 229–240.
[9] Y. Ju, B. Xu, *Proc. Combust. Inst.* 30 (2005) 2445–2453.
[10] B. Xu, Y. Ju, *Proc. Combust. Inst.* 31 (2007) 3285–3292.
[11] C.M. Miesse, R.I. Masel, C.D. Jensen, M.A. Shannon, M. Short, *AIChE J.* 50 (12) (2004) 3206–3214.
[12] C.M. Miesse, R.I. Masel, M. Short, M.A. Shannon, *Proc. Combust. Inst.* 30 (2005) 2499–2507.
[13] S. Prakash, A.D. Armijo, R.I. Masel, M.A. Shannon, *AIChE J.* 53 (6) (2007) 1568–1577.
[14] F. Richecoeur, D.C. Kyritsis, *Proc. Combust. Inst.* 30 (2005) 2419–2427.
[15] W.A. Sirignano, T.K. Pham, D. Dunn-Rankin, *Proc. Combust. Inst.* 29 (2002) 925–931.
[16] T.K. Pham, D. Dunn-Rankin, W.A. Sirignano, *Proc. Combust. Inst.* 31 (2007) 3269–3275.
[17] K. Maruta, J.K. Parc, K.C. Oh, T. Fujimori, S.S. Minaev, R.V. Fursenko, *Combust. Explos. Shock Waves* 40 (5) (2004) 516–523.
[18] K. Maruta, T. Kataoka, N.I. Kim, S. Minaev, R. Fursenko, *Proc. Combust. Inst.* 30 (2005) 2429–2436.
[19] S. Kumar, K. Maruta, S. Minaev, *Phys. Rev. E* 75 (1) (2007) 016208.
[20] S. Kumar, K. Maruta, S. Minaev, *Proc. Combust. Inst.* 31 (2007) 3261–3268.
[21] S. Kumar, K. Maruta, S. Minaev, *J. Micromech. Microeng.* 17 (4) (2007) 900–908.
[22] M. Wu, J. Hua, K. Kumar, *J. Micromech. Microeng.* 15 (2005) 1817–1823.
[23] A.W. Fan, S. Minaev, S. Kumar, W. Liu, K. Maruta, *Combust. Flame* 153 (3) (2008) 479–489.
[24] A.W. Fan, S. Minaev, S. Kumar, W. Liu, K. Maruta, *J. Micromech. Microeng.* 17 (10) (2007) 2398–2406.
[25] S. Minaev, K. Maruta, R. Fursenko, *Combust. Theory Model.* 11 (2) (2007) 187–203.
[26] S. Minaev, R. Fursenko, N. Bakirova, S. Kumar, K. Maruta, Proceedings of the Sixth Asia-Pacific

Conference on Combustion, Nagoya, Japan, 2007, p. 546.
[27] N.D. Bakirova, S.S. Minaev, R.V. Fursenko, Proceedings of the 13th International Conference on the Methods of Aerophysical Research, Part V, 2007, 9 pp.
[28] T.L. Jackson, J. Buckmaster, Z. Lu, D.C. Kyritsis, L. Massa, *Proc. Combust. Inst.* 31 (2007) 955–962.
[29] G. Pizza, C.E. Frouzakis, J. Mantzaras, A.G. Tomboulides, K. Boulouchos, *Combust. Flame* 152 (2007) 433–450.